Resubmitted to Acta Materialia in revised form, January 2022

Effects of aging on the stress-induced martensitic transformation and cyclic superelastic properties in Co-Ni-Ga shape memory alloy single crystals under compression

C. Lauhoff[a*], A. Reul[b], D. Langenkämper[c], P. Krooß[a], C. Somsen[c], M.J. Gutmann[d], B. Pedersen[e], I. Kireeva[f], Y.I. Chumlyakov[f], G. Eggeler[c], W.W. Schmahl[b], T. Niendorf[a]

[a] *Institut für Werkstofftechnik, Universität Kassel, Mönchebergstr. 3, 34125 Kassel, Germany*
[b] *Applied Crystallography, Department of Earth and Environmental Sciences, Ludwig-Maximilians-Universität, Theresienstr. 41, 80333 Munich, Germany*
[c] *Institut für Werkstoffe, Ruhr-Universität Bochum, Universitätsstr. 150, 44801 Bochum, Germany*
[d] *ISIS Facility, Rutherford Appleton Laboratory, Chilton, Didcot, Oxfordshire OX11 0QX, UK*
[e] *Heinz Maier-Leibnitz Zentrum (MLZ), Technische Universität München, Lichtenbergstr. 1, 85748 Garching, Germany*
[f] *Siberian Physical Technical Institute, Tomsk State University, Novosobornay Square 1, 634050 Tomsk, Russia*

**corresponding author. email: lauhoff@uni-kassel.de; phone: +49 561 804-3917; fax: +49 561 804-3662*

Co-Ni-Ga shape memory alloys attracted scientific attention as promising candidate materials for damping applications at elevated temperatures, owing to excellent superelastic properties featuring a fully reversible stress-strain response up to temperatures as high as 500 °C. In the present work, the effect of aging treatments conducted in a wide range of aging temperatures and times, i.e. at 300 – 400°C for 0.25 – 8.5h, was investigated. It is shown that

critical features of the martensitic transformation are strongly affected by the heat treatment conditions. In particular, the formation of densely dispersed γ'-nanoparticles has a strong influence on the martensite variant selection and the morphology of martensite during stress-induced martensitic transformation. Relatively large, elongated shaped particles promote irreversibility. In contrast, small spheroidal particles are associated with excellent functional stability during cyclic compression loading of ⟨001⟩-oriented single crystals. In addition to mechanical experiments, a detailed microstructural analysis was performed using *in situ* optical microscopy and neutron diffraction. Fundamental differences in microstructural evolution between different material states are documented and the relations between thermal treatments, microstructure and functional properties are explored and rationalized.

Keywords: Shape memory alloys (SMAs); aging; nanoparticles; neutron diffraction; martensite variant selection

1. Introduction

Shape memory alloys (SMAs) have been intensively studied for decades [1],[2]. So far, the most widely employed SMA system is binary Ni-Ti being well known from biomedical applications such as orthodontic wires or stents. Ni-Ti is highly biocompatible, can be processed into various semi-finished products such as wires, tubes or sheets, and features excellent functional properties. Still, the inherent application temperature limit (80 °C) hinders its technological breakthrough in high-temperature applications, e.g. in the aerospace and energy sector or chemical industry, where operating temperatures often exceed 100 °C [1]–[5].

Heusler-type Co-Ni-Ga alloys constitute a class of ferromagnetic SMAs (FSMAs) undergoing a thermoelastic MT from a cubic B2-ordered austenite to a non-modulated tetragonal $L1_0$-martensite [6],[7]. Initially developed to provide for an alternative to Ni_2MnGa [8],[9], which suffers extreme brittleness, Co-Ni-Ga recently received attention due to its outstanding functional properties at elevated temperatures. In single-crystalline state, a fully reversible stress-induced martensitic transformation (SIMT) up to temperatures as high as 500 °C [10]–[12] and excellent cyclic stability without any traces of functional degradation up to 100 °C [13],[14] have been reported under both compressive and tensile loading. Owing to a pronounced anisotropy of the MT and a limited number of martensite variants during cubic to tetragonal transformation, polycrystalline structures with random texture suffer transformation-induced constraints at grain boundaries. Thus, premature failure upon thermo-mechanical loading and/or processing is commonly observed hindering any industrial usage of Co-Ni-Ga SMAs so far [15],[16]. However, substantial progress in terms of robust processing of Co-Ni-Ga via thermo-mechanical routes [16]–[18] and additive

manufacturing [19],[20] has been made very recently. Employing hot extrusion [18] and directed energy deposition (DED) technique [20], excellent functional properties can be attained through process-induced formation of oligocrystalline and highly textured columnar-grained microstructures, respectively. In addition to direct microstructure design by adequate control of process-related parameters [17],[19], TTs can be controlled in the Co-Ni-Ga system in a wide temperature range by choice of appropriate heat treatment procedures [21]–[23]. For instance, aging of stress-induced martensite, referred to as *SIM-aging*, is suited to directly tailor the TTs based on changes in chemical order [22],[24]–[26]. Thereby, Co-Ni-Ga alloys possess great potential for high-temperature actuation and damping applications.

Low- and intermediate-temperature aging treatments in the austenitic phase promote precipitation of the ordered face-centered cubic (fcc) γ'-phase ($L1_2$) [27]. The significant influences of such fine dispersed γ'-nanoparticles on SME and SE (i.e. TTs and transformation strains, thermal and stress hysteresis, and the temperature range for SE), on the thermally and stress-induced B2-$L1_0$ MT and on magnetic domain structures in Co-Ni-Ga SMAs have been already reported [23],[28]–[33]. As demonstrated by Kireeva et al. [30], precipitation-hardening of the austenitic B2-matrix is effective to provide for a further improvement of the functional properties at elevated temperatures, i.e. an enlargement of the SE window. However, the microstructure of the martensitic phase strongly depends on size and shape (spheroidal or elongated) of the coherent particles. A drastic reduction in twin thickness of thermally induced martensite was reported with increasing particle size [31]. Once a critical size is exceeded, difficulties in accommodating the transformation strain around the non-transforming particles promote additional nano-twinning of the martensitic

phase. This micromodulation strongly contributes to irreversible processes during MT [30],[31]. In turn, large elongated particles of one single orientation (aging under superimposed stress) have been proven to be advantageous for the functional performance compared to their non-preferentially oriented counterparts. Within the well-defined stress fields around the oriented particles the accommodation of martensite is improved suppressing the structural micromodulation [30]. Furthermore, as evidenced by *in situ* optical microscopy and neutron diffraction analysis, the presence of γ'-particles strongly affects the martensite variant selection and the morphology of stress-induced martensite. Whereas a single, internally twinned martensite is present in the solution-annealed (precipitate-free) condition, coherency stress fields existing around γ'-particles with spheroidal shape induce a multi-variant microstructure characterized by pronounced phase boundary interactions [33]. However, the effect of nanoparticles on the SIMT as a function of particle size and shape, as already detailed for thermally induced martensite [31], has not been reported so far. For further progress in the field of SMAs and for their successful incorporation into envisaged applications, a thorough understanding of the mechanisms leading to changes of the stress-strain response during cyclic loading is one of the key issue that needs to be addressed. Cyclic deformation causes a decrease in the critical stress level for the onset of the SIMT, a decrease in stress hysteresis and accumulation of irreversible strains, as numerously shown in Ni-Ti. This evolution of the transformation characteristics is attributed to the introduction and accumulation of dislocations in the course of cycling, i.e. induced by dislocation-slip [34]–[39]. Therefore, microstructural strengthening of the austenitic matrix by either grain refinement in polycrystalline material [37],[39] or introduction of optimized

nanoparticles [35],[36] to increase the critical stress level for slip has been reported to result in significantly improved cyclic stability.

In the Co-Ni-Ga system, functional fatigue of single crystalline material under SE loading was already comprehensively investigated. The crystallographic orientation, stress states, training procedures and test temperatures were in focus of these investigations [10],[13],[14],[40]. Diffusion-controlled mechanisms, e.g. changes in the degree of chemical order, dictate cyclic instabilities at temperatures above 300 °C [10],[40]. In the temperature range below 300 °C, in turn, changes in the stress-strain characteristics are mainly triggered by dislocation activity during the SIMT [13],[14]. In this regard, the crystallographic orientation governs the cyclic stability of Co-Ni-Ga alloys to a large extend. While ⟨001⟩-oriented single crystals feature excellent resistance against cyclic degradation, samples with ⟨123⟩ orientation suffer a rapid degradation of the transformation characteristics under cyclic loading. These differences can be related to the active slip systems and related values of the resolved shear stress factor (RSSF) [14]. Furthermore, a distinctive tension-compression asymmetry in the superelastic cyclic stress-strain response was shown. More rapid functional degradation was observed in compression. This was attributed to the number of active martensite variants and pronounced martensite variant-variant interactions under compressive loading, leading to severe dislocation activity [13].

As detailed for the Ni-Ti system, precipitation-hardening is a promising venue to minimize functional degradation, since dislocation slip characteristics can be modified by secondary phases [36]. However, it has not been investigated yet in how far either the strength-enhancing effect [30] or the complex multi-variant microstructure, which is caused by nanometric precipitates [33], dominate the cyclic properties in the Co-Ni-Ga system. No

studies are available in open literature detailing the functional fatigue behavior of a precipitation-hardened condition in this system. Therefore, the present paper investigates the SE cyclic deformation behavior of aged Co-Ni-Ga.

2. Material and experimental methods

Ingots of Co-Ni-Ga with a nominal chemical composition of 49Co-21Ni-30Ga (in at.%) were prepared using vacuum induction melting. The chosen chemical composition is designed for enhanced functional properties, i.e. a high degree of strain recoverability [12]. Large single crystals with sizes up to several centimeters were grown by the Bridgeman technique under helium inert gas atmosphere. For compression tests, cuboidal samples with dimensions of 3 x 3 x 6 mm^3 were electro-discharged machined (EDM) from the bulk single crystals such that their longer (i.e. loading) axes coincided with ⟨001⟩ of the austenitic phase, while normal vectors of the lateral surfaces were parallel to ⟨100⟩ and ⟨010⟩. The ⟨001⟩ crystal direction was selected, since plastic deformation is strongly curtailed owing to the ⟨001⟩{011} type slip systems in B2-ordered alloys [41]. Thus, the effect of dislocation activities on the transformation behavior is minimized in present work. Furthermore, the use of single crystals instead of polycrystalline material allowed for a systematic assessment of the operant microstructural mechanisms. Crystallographic orientations of the bulk crystals for machining purposes were determined using X-ray diffraction. Following EDM, samples were ground down to remove any residue from processing. In order to obtain a single phase condition free of any secondary phases [31],[33], all samples were initially solution-annealed at 1200 °C for 12 h. Solution-annealing was conducted in sealed quartz glass tubes under argon atmosphere to avoid oxidation and Ga evaporation, followed by breaking manually the quartz

tubes at ambient conditions. Using differential scanning calorimetry (DSC) transformation temperatures were determined (not shown). The solution-annealed state is characterized by martensite finish (M_f), martensite start (M_s), austenite start (A_s) and austenite finish (A_f) temperatures of -10, -6, 11 and 14 °C, respectively. Subsequently, the solution-annealed samples were given aging treatments in a wide temperature and time range. Aging was performed at temperatures of 300, 350 and 400 °C for 0.25, 1, 3 and 8.5 h, respectively. Aging parameters were chosen in accordance to Refs. [22],[30]–[32].

Monotonic and cyclic quasi-static uniaxial compression tests were carried out on a servohydraulic test rig equipped with a digital microscope and a tele-zoom objective for *in situ* OM analysis. Fig. 1 introduces the nomenclature of the SE parameters used for quantitative analysis of the transformation characteristics. Tests were run at 100 °C in displacement control at a nominal strain rate of 1×10^{-3} s^{-1}. Each SE stress-strain cycle was performed up to a preset maximum strain of -5% upon loading and a given minimum load of -200 N for unloading. The maximum strain level was set to -5% with respect to the theoretical transformation strain in compression for the ⟨001⟩ crystal direction [14]. Heating of the samples was conducted by controlled convection furnaces. Temperatures were measured with a thermocouple directly attached to one of the lateral sample surfaces. The test temperature was chosen for ease of comparison with data previously reported for the solution-annealed, i.e. precipitate-free, condition [33]. Strain measurement was realized using a high-temperature extensometer with a gauge length of 12 mm. Its ceramic rods were directly attached to the compression grips, which were treated as absolutely rigid for calculation of the nominal strain.

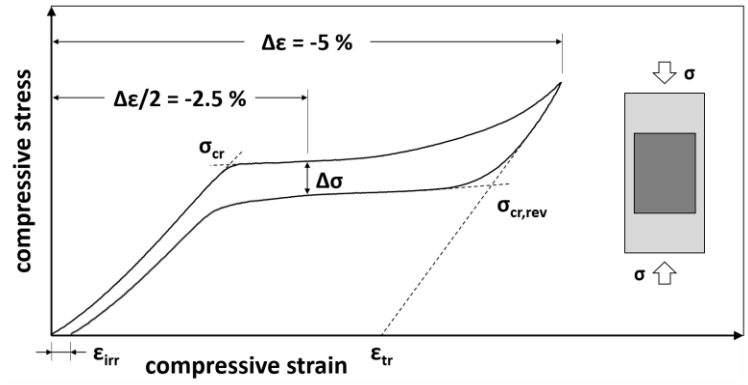

Figure 1: Schematic detailing the terminology used to assess the SE response: Critical stress levels for the onset of the stress-induced forward (σ_{cr}) and reverse transformation ($\sigma_{cr,rev}$) were evaluated using the intersecting slope lines method. The width of stress hysteresis ($\Delta\sigma$) was measured at half of the applied strain amplitude ($\Delta\varepsilon$), i.e. at -2.5%. The transformation strain and the irrecoverable strain within a stress-strain cycle are named ε_{tr} and ε_{irr}, respectively. The inset sketches a compression sample with a dark gray shaded area indicating the sample surface area from where the in situ optical micrographs (Figure 6) were recorded.

In situ OM as well as neutron diffraction experiments were carried out to shed light on microstructural characteristics of the SIMT. For the *in situ* OM analysis, surface images of a representative area up to 2.3 x 3.0 mm^2 (cf. inset in Fig. 1) were captured at various stages of the stress-strain curves. In addition to the standard silicon carbide grinding down to a grit size of 5 µm, the lateral surfaces investigated were mechanically polished using a colloidal SiO_2 suspension with 0.02 µm particle size.

In situ neutron diffraction was conducted on preliminary tested samples (used for *in situ* OM) with the single crystal Laue diffractometer SXD [42] at ISIS neutron source, Rutherford Appleton Laboratory, Oxfordshire. In accordance with the *in situ* OM

experiments, the SE tests were run at 100 °C in displacement control at a nominal strain rate of 1 x 10^{-3} s^{-1} using a miniature load frame (Kammrath & Weiß GmbH, Germany). Heating of the samples was conducted using a cartridge heating system. The cartridge heaters were attached to sample holders. Temperatures were double-checked in reference tests to ensure a homogeneous temperature distribution within the entire sample. During each loading stage, diffraction data were recorded for 30 min in the austenitic and 175 min in the dual-phase austenitic/martensitic or fully martensitic condition, respectively. Strains at each loading stage were deduced from stress values obtained from the previously conducted *in situ* OM experiments. Neutron diffraction allows to probe sample volumes of several mm^3 due to the high penetration depth of neutrons into matter (e.g. 20 mm into steel or 100 mm into aluminum) [43]. SXD uses time-of-flight (TOF) technique employing a polychromatic neutron beam with incident wavelengths in the range of 0.2-10 Å. The orders of a given Bragg reflection (e.g. 200, 400, 600) are collected at different TOF. For a given scattering angle 2θ and total neutron flight path distance from spallation target to the detector, TOF is proportional to crystal spacing d. Neutrons scattered within the sample volume are collected on eleven position-sensitive LiF/ZnS scintillator area detectors arranged around the sample position. This setup allows to collect complete diffraction patterns of large 3D volumes within in a wide range of reciprocal space leading to increased speed of data collection compared to monochromatic single crystal neutron diffractometers. A complete diffraction pattern as well as details on the detector arrangement of SXD are provided in the supplementary material. For further details on the *in situ* setup of SXD being used in the present study the reader is referred to [6]. For analysis of the diffraction data, Bragg reflections on the area detectors were integrated and plotted as 1D-line patterns over

d-spacing range. For the sake of brevity, only 1D-line patterns obtained from detector 1 (cf. supplementary material, Fig. S-1) will be shown (Fig. 7). Diffraction data were indexed and integrated using the software package SXD2001 [42].

Microstructural analysis was conducted using a FEI Tecnai F20 transmission electron microscope (TEM) operated at a nominal accelerating voltage of 200 kV. Small discs were sliced perpendicular to the ⟨001⟩ crystal direction of the austenite and mechanically ground down to 0.15 µm thickness. Finally, electron transparent areas were obtained via twin-jet electropolishing using a perchloric acid solution containing 60 ml perchloric acid, 340 ml butanol and 600 ml methanol.

3. Experimental results

3.1 Superelastic behavior

Data detailing the mechanical behavior of precipitation-hardened Co-Ni-Ga SMA in open literature are scarce and limited to aging treatments at ~ 350 °C for up to 3 h [30]–[33]. Fig. 2 presents monotonic SE responses of ⟨001⟩-oriented $Co_{49}Ni_{21}Ga_{30}$ single crystals aged in a wide range of aging temperatures and times, i.e. at 300, 350 and 400 °C for 0.25, 1, 3 and 8.5 h, respectively. In line with the solution-annealed reference material (recompiled from [33] and plotted using dashed lines in Fig. 2), the compressive stress-strain curves obtained at 100 °C demonstrate perfect SE responses with full strain recovery being almost independent of the aging treatment. Only following long-time aging and/or higher aging temperatures, i.e. 8.5 h at 350 °C as well as 3 and 8.5 h at 400 °C, the aged crystals exhibit irrecoverable strains (ε_{irr}) up to 0.5% upon unloading from the maximum applied strain of -5%. Nonetheless, it is obvious from Fig. 2 that the aging parameters have a significant

influence on the shape of the stress-strain hysteresis. A detailed analysis of the monotonic SE properties (for definitions see Fig. 1) is provided in the supplementary material. For brevity, in the remainder of the paper emphasis is primarily on the functional properties under cyclic loading.

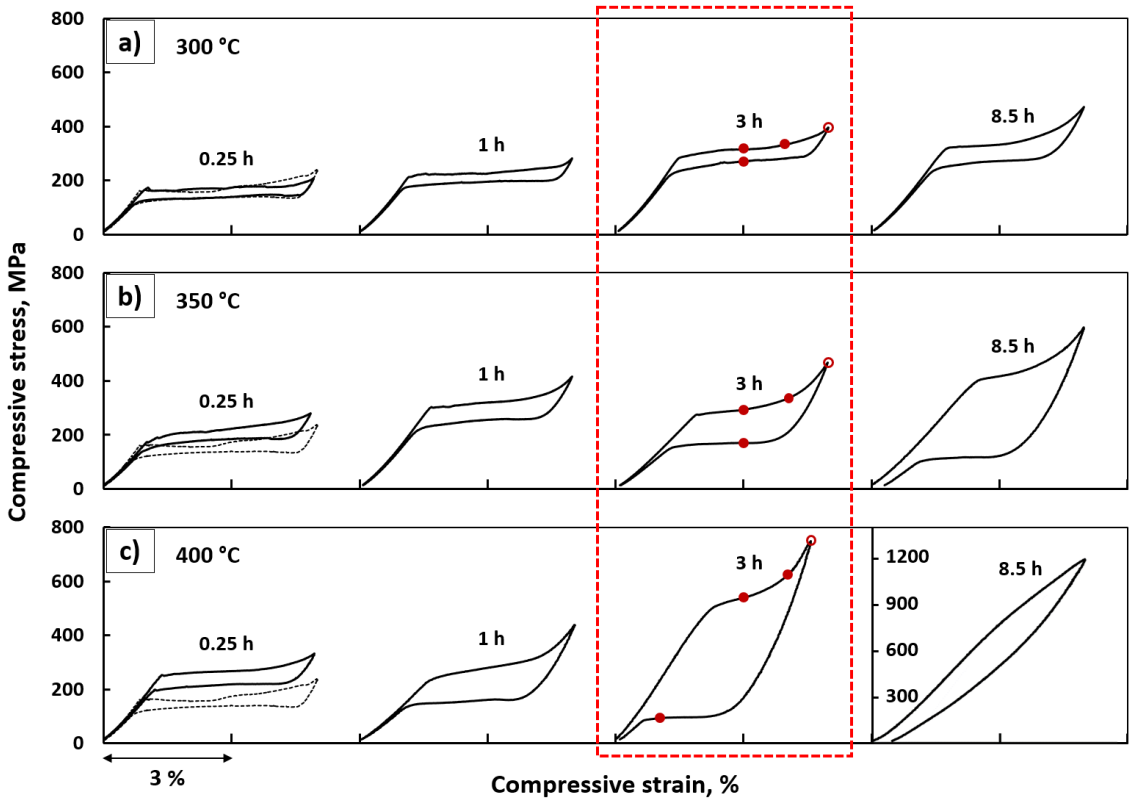

Figure 2: Characteristic superelastic stress-strain hysteresis under compressive load at 100 °C of ⟨001⟩-oriented $Co_{49}Ni_{21}Ga_{30}$ single crystals aged 0.25, 1, 3 and 8.5 h at 300 °C (a), 350 °C (b) and 400 °C (c), respectively. The reference solution-annealed, i.e. precipitate-free, condition recompiled from [33] is plotted using dashed lines. Specific stress-strain stages being subsequently characterized via in situ OM and neutron diffraction are marked by red points and circles, respectively.

Fig. 3 shows compressive cyclic SE responses of ⟨001⟩-oriented single crystals in selected heat treatment conditions obtained at 100 °C. Results are shown for crystals aged at 300, 350 and 400 °C for 3 h (for better readability 300, 350 and 400 °C in the reminder of the text) marked by the dashed red frame in Fig. 2. Among the heat treatment conditions studied in present work (Fig. 2), these material states were chosen as the corresponding results were found to reveal the most pronounced differences with respect to the values of the SE parameters, the aging-induced microstructural features and the SIMT behavior (cf. Figs. 2 and 3, chapters 3.2 and 3.3, respectively). Thus, based on direct comparison of these conditions, the correlation between the functional properties and the microstructural mechanisms is most obvious. In addition, in Fig 3 results for the solution-annealed reference state are included, since data in open literature detailing the cyclic stability of the transformation behavior in ⟨001⟩-oriented Co-Ni-Ga are limited to the as-grown condition so far [13],[14].

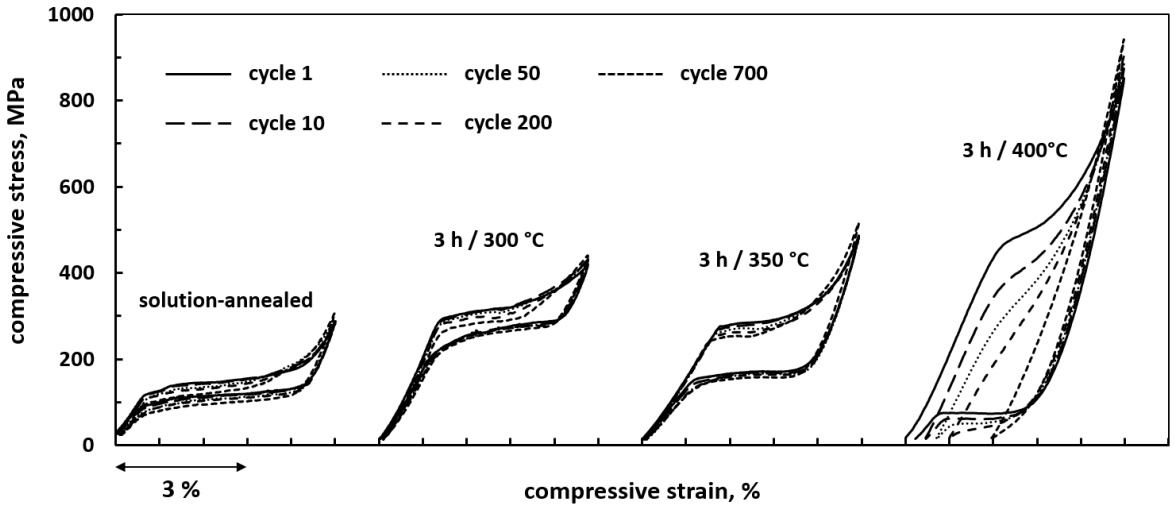

<u>Figure 3:</u> Characteristic superelastic cyclic stress-strain responses under compressive load at 100 °C of ⟨001⟩-oriented $Co_{49}Ni_{21}Ga_{30}$ single crystals in the solution-annealed condition and after aging for 3 h at 300, 350 and 400 °C, respectively.

It is obvious from Fig. 3 that the performed heat treatment strongly affects the stability of the stress-strain response. Here, it has to be emphasized that the aged crystals are the same samples previously probed by the single cycle test shown in Fig. 2. Thus, the 1st fatigue cycle presented in Fig. 3 is actually the 2nd overall cycle of the aged samples. The macroscopic transformation behavior of the solution-annealed as well as 300 and 350 °C aged crystals remains relatively stable in the course of cycling. Only minor changes of the shape related to the stress-strain hysteresis can be observed. In contrast, cyclic loading of the sample aged at 400 °C results in a pronounced change of the transformation behavior revealing an almost complete loss of SE. Thus, all cyclic experiments were stopped after 700 cycles.

In order to quantitatively assess the stability of the stress-strain behavior upon cycling following a particular heat treatment, the evolution of SE parameters closely related to the degradation behavior of SMAs are elaborated and plotted as a function of cycle number in Fig. 4. The change of both σ_{cr} and $\Delta\sigma$ in relation to the 1st cycle of the cyclic experiments is shown in Fig. 4a and b, respectively. Following an initial "rapid" decrease of σ_{cr} in the early stages of cycling (1 to 100 cycles), the reduction of σ_{cr} slows down or even reaches saturation with further cycling. After 700 cycles, the decrease is accumulated to -19, -26 and -34 MPa for the solution-annealed, 300 and 350 °C aged condition, respectively. By contrast, σ_{cr} continually decreases by -276 MPa within the first 200 cycles following aging at 400 °C. Subsequently, a reliable evaluation of the SE parameters is not possible based on the hysteresis obtained. Hence, data points for cycle numbers above 200 of the condition aged at 400 °C are not plotted in Fig. 4a and b. For this particular condition, the decrease in σ_{cr} strongly affects the change of $\Delta\sigma$ from cycle to cycle (Fig. 4b), as the critical stress for the

reverse transformation ($\sigma_{cr,rev}$) remains nearly unchanged upon cycling (cf. Fig. 3). In contrast, the solution-annealed sample is characterized by hardly any change of $\Delta\sigma$ (-4 MPa) after 700 SE cycles. A slight decrease by -12 and -14 MPa can be observed for the 300 and 350 °C aged single crystals. In summary, the solution-annealed condition is characterized by the highest degree of cyclic stability among the heat treatments studied, while the susceptibility to degradation steadily increases with aging temperature. Nonetheless, even the 300 and 350 °C aged single crystals reveal a high resistance against cyclic degradation being similar to the solution-annealed condition.

Another quantitative measure of the cyclic degradation resistance is the accumulation of irrecoverable strains (ε_{irr}) at a given cycle number. During testing a constant absolute strain limit of -5% was used. Thus, the contributions of strain linked to the phase transformation and the elastic deformation of austenite changed from sample to sample due to variations in σ_{cr} (cf. Fig. 3). For better comparability, the accumulated permanent strains at each SE cycle are shown normalized to the initial transformation strain ($\varepsilon_{tr}^{N=1}$) versus number of cycles in Fig. 4c. The Co-Ni-Ga crystals in the solution-annealed condition and aged at 300 and 350 °C feature excellent recoverability upon cycling with marginal normalized accumulated permanent strains of 0.04, 0.03 and 0.02 after 700 cycles, respectively. By contrast, in the case of the 400 °C aging treatment a continuous rapid permanent strain accumulation to a final value of 0.70 is found eventually indicating a fully degraded condition. In order to gain insights into the microstructural mechanisms being responsible for the differences with respect to the SE properties, systematic TEM analysis as well as *in situ* OM and neutron diffraction experiments have been conducted and will be detailed in the following.

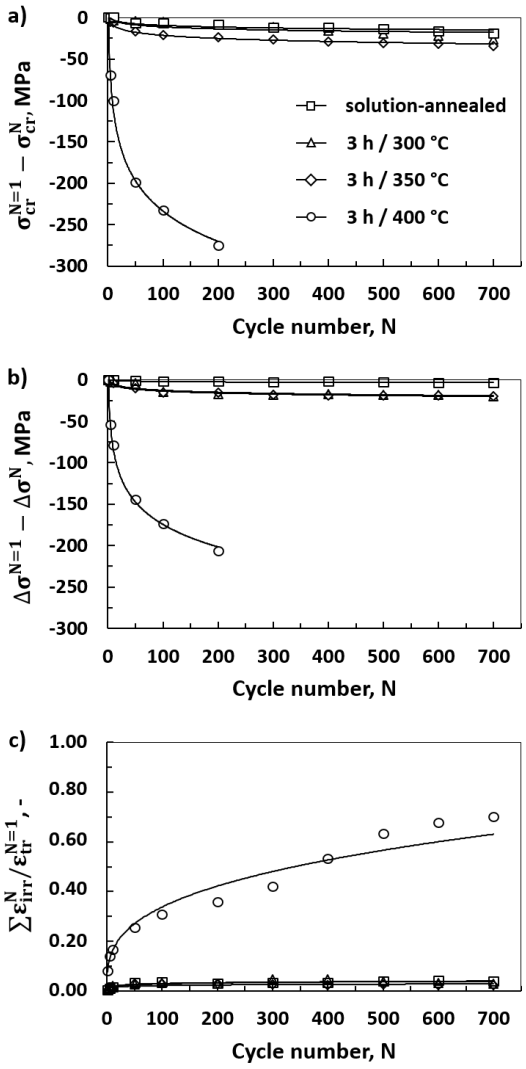

<u>Figure 4:</u> Evolution of superelastic parameters versus cycle number of $Co_{49}Ni_{21}Ga_{30}$ single crystals in the solution-annealed condition and after aging for 3 h at 300 °C, 350 °C and 400 °C, respectively: $\sigma_{cr}^{N=1} - \sigma_{cr}^{N}$ (a), $\Delta\sigma^{N=1} - \Delta\sigma^{N}$ (b) and $\sum\varepsilon_{irr}^{N}/\varepsilon_{tr}^{N=1}$ (c). Data points were extracted from the experiments in Fig. 3. In (a) and (b), values for the 400 °C aged condition could only be evaluated up to the 200th cycle. See main text for details.

3.2 TEM microstructure analysis of $Co_{49}Ni_{21}Ga_{30}$ crystals following aging treatments

Fig. 5 shows characteristic microstructures of Co-Ni-Ga crystals subjected to aging treatments conducted for 3 h. Following 300 °C aging, the TEM analysis reveals a single phase microstructure as also seen after solution-annealing at 1200 °C (not shown). As can be deduced from the selected area electron diffraction (SAED) patterns in Fig. 5a, the 300 °C aged condition is fully austenitic featuring B2-type ordering, as indicated by the superlattice reflection spots. On the contrary, after aging at 350 and 400 °C, the SAED patterns obtained from the $[001]_{B2}$ zone axes reveal extra spots between the 020_{B2}- and 200_{B2}-type reflections (marked by the white arrows in Fig. 5b and d), respectively. The patterns can be indexed as a superposition of the austenitic B2-phase and γ'-phase having an $L1_2$-ordered fcc unit cell. This precipitation behavior is fully consistent with data shown in literature [7],[22],[31]. Kireeva et al. [31] reported that significant amounts of γ'-particles precipitates evolve upon short time aging at a temperature of 350 °C. At 300 °C, secondary phase particles were only found following long-time aging treatments, namely at least 8.5 h [7],[22].

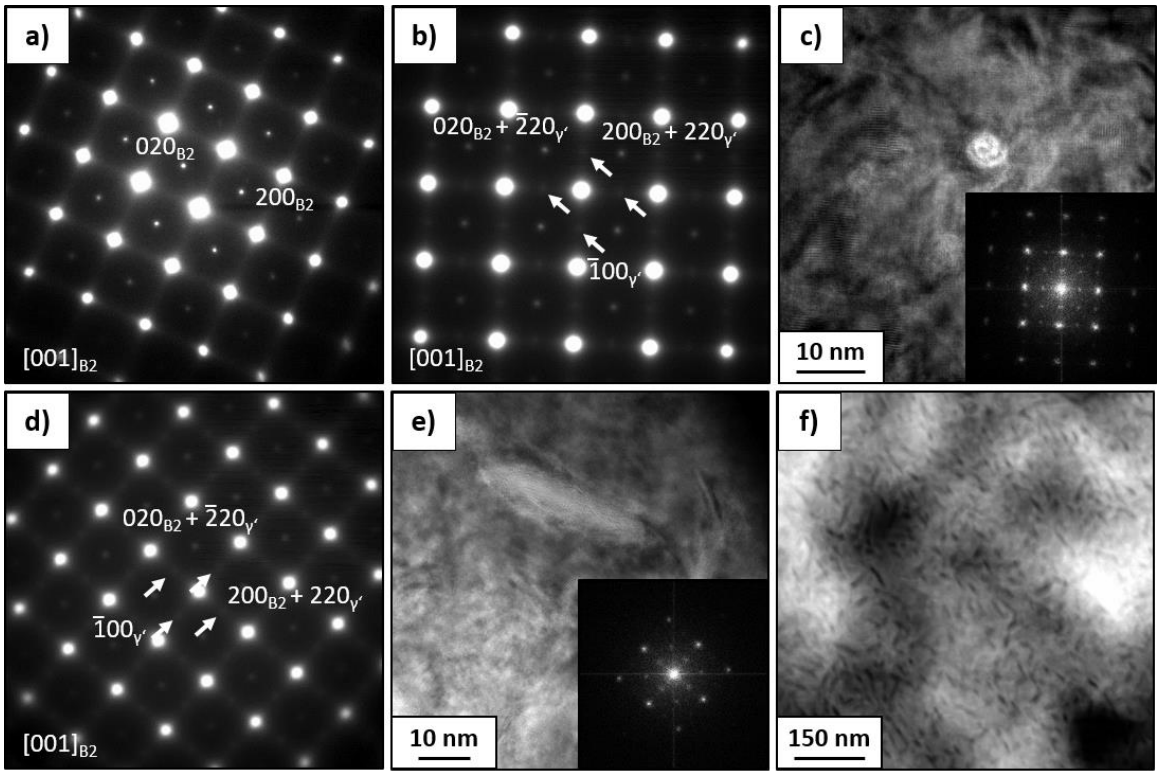

<u>Figure 5:</u> TEM analysis of $Co_{49}Ni_{21}Ga_{30}$ crystals revealing the characteristic microstructures after 3 h aging treatments at 300 °C (a), 350 °C (b, c) and 400 °C (d-f), respectively. The SAED patterns (a, b, d) shed light on the presence of the secondary γ'-phase (if existent, marked by white arrows). The HR-TEM (c, e) and STEM (f) images reveal the morphology (size and shape) and orientation of the γ'-particles, respectively. See text for details.

Sizes and shapes of individual particles ($L1_2$, as revealed by the fast Fourier transformation (FFT) patterns (insets in Fig. 5c and e)) are illustrated by the high-resolution transmission electron microscopy (HRTEM) images in Fig. 5c and e. After the 350 °C aging the γ'-particles are characterized by a spheroidal shape with diameters up to 10 nm (Fig. 5c). By increasing the aging temperature to 400 °C the particles grow in size and change their shape

from spheroidal to elongated. Particles are up to 10 nm in width and 40 nm in length featuring an aspect ratio of up to 4 (Fig. 5e). In addition, as can be deduced from the scanning transmission electron microscopy (STEM) image in Fig. 5f, the elongated particles are not randomly oriented. Generally, austenitic matrix and the precipitate crystal lattice retain fixed orientation relationships. In the Co-Ni-Ga system, the γ'-phase precipitates exhibit {111}-type habit planes [30]. Thus, according to previous studies [30],[44], the precipitation of four orientations of variants of the elongated γ'-particles with habit planes on the four equivalent $\{111\}_{B2}$-type planes is assumed to be present after aging at 400 °C. However, it should be mentioned that only two different traces of orientation variants being inclined by about ±45° to the horizontal are visible in Fig. 5f. This is due to the fact that each trace represents two different particle variants, which are indistinguishable from each other in this particular cross section. The elongated or needle-like shape being existent following the 400 °C aging is the typical morphology of the γ'-phase upon segregation at higher temperatures, i.e. close to the equilibrium conditions [23],[30],[45].

3.3 In situ optical microscopy and neutron diffraction analysis of the stress-induced martensite

Systematic *in situ* OM studies have been conducted at different load stages of the stress-strain curves marked by the red points in Fig. 2 (markings are included for the sake of clarity). For the *in situ* experiments, a new set of untested aged samples was used. The characteristic stress-strain responses of the *in situ* samples are not shown here, as these are perfectly in line with the corresponding hysteresis curves depicted in Fig. 2. Fig. 6 displays the microstructures of the ⟨001⟩-oriented Co-Ni-Ga single crystals aged at 300, 350 and 400 °C.

The micrographs were recorded for the SE curves obtained at 100 °C during loading (a-i) and unloading (j-l). Loading direction (LD) is horizontal as illustrated in Fig. 6c. In general, both the forward and reverse SIMT are characterized by a lamellar martensitic microstructure. The martensite plates, which can be distinguished from the austenitic parent phase by the obvious material contrast, are known as habit plane variants (HPVs) owing to their direct interface with the austenitic matrix. The martensite within the HPVs comprises two twin-related domain variants (correspondent variant pair, CVP) being separated by twin boundaries [14],[40],[46]. The martensite domain variants are not visible at the mesoscopic scale employing OM. These structures will be detailed hereafter based on the neutron diffraction results, as for example highlighted by the schematic shown in Fig. 7.

The micrographs of the aged conditions recorded at -3% applied compressive strain (forward SIMT) are shown in Fig. 6a-f. In all single crystalline states, the phase transformation proceeds by simultaneous formation of numerous interfaces, i.e. multiple small martensite plates coexist with the untransformed austenite. Here, the different aging treatments obviously affect the transformation behavior in terms of the HPV selection as well as the morphology of the stress-induced martensite. During the forward SIMT, Fig. 6a and b show that both the 300 and 350 °C aged crystals are clearly characterized by the formation of HPVs with two different orientations regarding LD (marked as HPV_A and HPV_B in Fig. 6d). From the intensity distributions obtained from neutron diffraction and shown in Fig. 7 it is deduced that martensite plates (HPVs), which feature the same orientation with respect to LD, consist of the same CVP (as will be discussed in a following paragraph). Between these various moving phase boundaries severe interaction can be seen. These interactions lead to the local evolution of distorted and misaligned habit planes. In particular, this phenomenon can be

observed in areas, where the differently oriented HPVs are in direct contact. As can be deduced from the micrographs recorded with higher magnification at -3% (Fig. 6d, e), the degree of interactions and the distortions of habit planes are more pronounced following the 350 °C aging (area marked by the dashed circle in Fig. 6e).

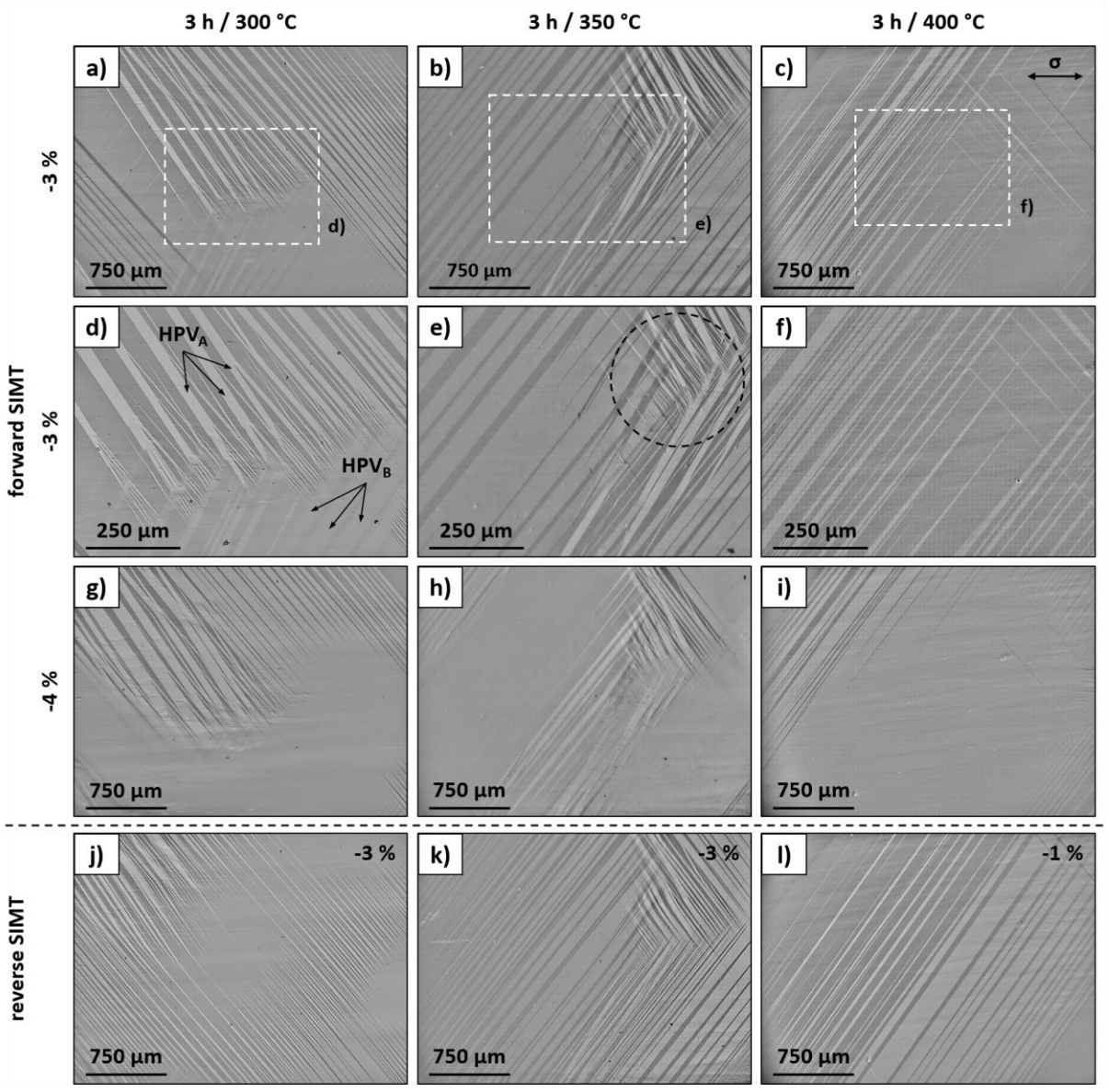

Figure 6: In situ OM analysis of ⟨001⟩-oriented $Co_{49}Ni_{21}Ga_{30}$ single crystals aged 3 h at 300 °C (a, d, g, j), 350 °C (b, e, h, k) and 400 °C (c, f, i, l), respectively. The micrographs depict a lateral {100}-surface. Data were recorded during single cycle tests at 100 °C under

compression. (a-f) -3% strain upon loading, (g-i) -4% strain upon loading, (j-l) unloading with strain level indicated on the micrograph. Loading direction is marked in the upper right corner of image (c). See main text for details.

In contrast to the twofold HPV configuration upon 300 and 350 °C aging (except for some phase fronts in the upper right corner of Fig. 6c and f), the 400 °C aged Co-Ni-Ga sample is predominantly characterized by the evolution of HPVs of a single orientation. Thus, only minor variant-variant interactions occur and HPVs with well-defined habit planes are present. However, the amount of nucleated phase fronts and the thickness of the individual martensite plates seems to vary with respect to the heat treatment (cf. Fig. 6a-c), i.e. the 400 °C aging leads to a further refinement of the martensitic microstructure compared to the aging treatments at 300 and 350 °C and the solution-annealed condition [33]. Further loading of the samples to -4% (Fig. 6g-i) results in growth of martensite via concurrent thickening of the individual martensite plates. The HPV selection is not altered with increasing straining. Final straining within a SE cycle to the maximum strain value of -5% leads to a fully martensitic microstructure. As it is hard to differentiate between the individual plates in OM, the final loading stage will only be assessed by neutron diffraction (cf. Fig. 7).

Fig. 6j-l show micrographs recorded at -3 and -1% applied compressive strain during reverse SIMT. Due to the significantly lower value of $\sigma_{cr,rev}$ (cf. Fig. 2), the microstructure of the 400 °C aged sample is depicted at -1% to allow for direct comparison to the transformation states of the 300 and 350 °C aged conditions. For all aging conditions, the martensite becomes unstable upon unloading and the reverse transformation to austenite sets in. This is accompanied by the nucleation of numerous phase fronts in all cases. The habit planes of

these phase fronts are parallel to the ones observed during forward SIMT. Consequently, it can be deduced that both the reverse and forward SIMT proceed in a very similar manner. Interestingly, unlike the formation of two HPV systems upon loading, the reverse SIMT of the 300 °C aged sample is characterized by HPVs with only a single orientation (the one that has been dominant (HPV_A) during the forward transformation (cf. Fig 6a, j)). In contrast, the HPV selection has not been changed in the samples aged at 350 and 400 °C. Optical micrographs at additional strain levels upon unloading are not shown here as no further information could be gained.

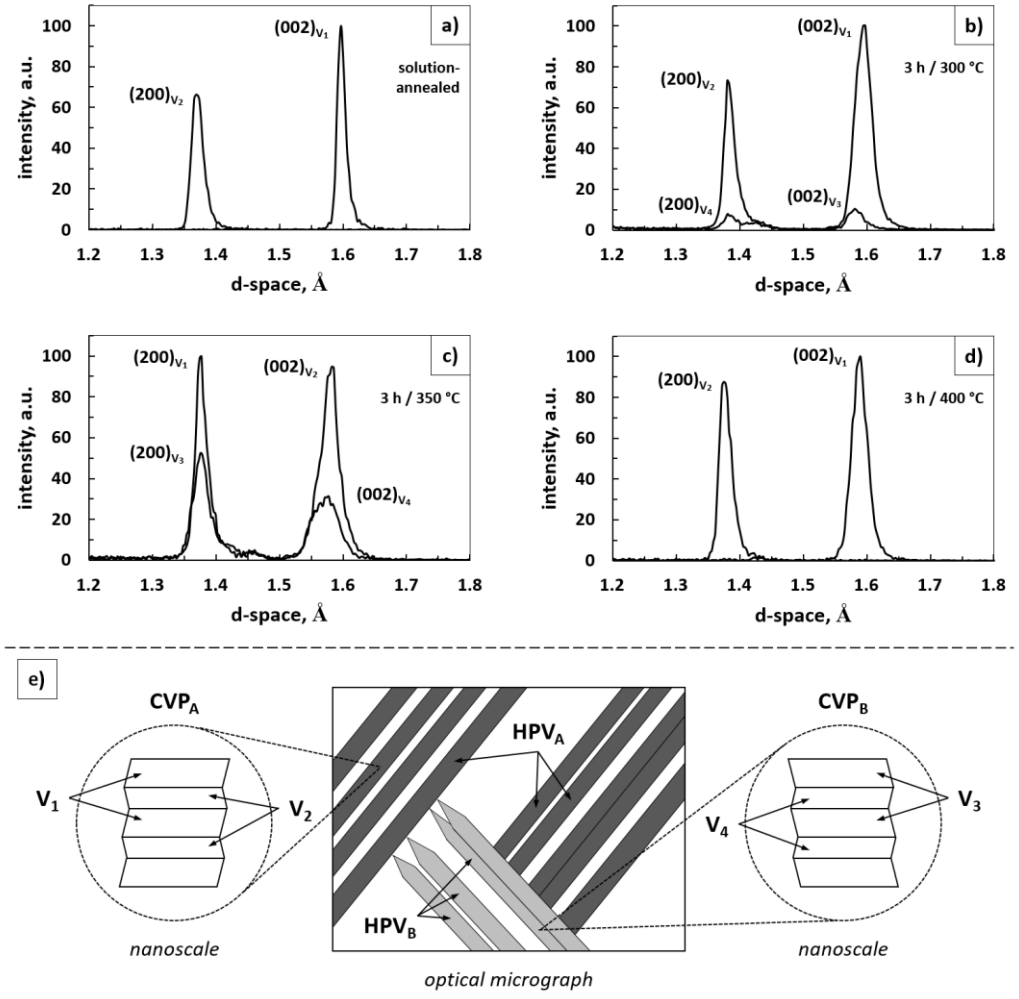

Figure 7: In situ TOF neutron diffraction analysis of ⟨001⟩-oriented $Co_{49}Ni_{21}Ga_{30}$ single crystals in the solution-annealed condition (a) and after aging for 3 h at 300 °C (b), 350 °C (c) and 400 °C (d), respectively. Diffraction data show intensities as a function of d-spacing (1.2 – 1.8 Å) recorded during single cycle tests at 100 °C under compression at -5 % applied strain. The martensite variant selection is illustrated by the indexed and labeled diffraction peaks for the stress-induced martensite domain variants (V_1 – V_4). The schematic (e) depicts the most relevant relationships on the nano- and mesoscopic scale between these domain variants, the CVP systems and the types of HPVs observed in the heat treatment conditions. See main text for details.

As can be deduced from the results shown in present work and in line with data shown in literature, OM analysis is an appropriate method to illustrate the morphology of the stress-induced martensitic phase, i.e. number and characteristics of the interfaces and the degree of HPV interactions. Further insights could be obtained by application of synergetic techniques such as digital image correlation (DIC) for assessment of evolution of local strains [47],[48]. However, as has been detailed in studies available, some details being of major interest of present work, i.e. martensite morphology and variant selection on the sample surface, cannot be assessed when relatively large sample volumes are probed due to the limitations of DIC [40]. Thus, follow-up studies will have to consider multi-scale DIC approaches to provide for quantitative assessment of evolution of local strains. Neutron diffraction has been proven to be a valuable technique for an in-depth phase analysis providing structural information from bulk samples [25],[49]. As shown in literature for numerous SMAs, phase quantification of martensite domain variants as well as elementary deformation mechanisms,

such as twinning processes, can be elaborated [6],[33],[50]–[53]. Therefore, *in situ* TOF neutron diffraction experiments have been conducted in present work in order to shed light on martensite variant selection and volume ratios of the individual domains. The aged samples previously probed via *in situ* OM (Fig. 6) were investigated in a second SE single cycle test at 100 °C at the ISIS neutron source. Data were recorded in the unloaded condition before testing and at the maximum compressive strain level imposed during the stress-strain cycles. In addition, neutron diffraction analysis of solution-annealed ⟨001⟩-oriented single-crystalline Co-Ni-Ga, i.e. the precipitate-free reference state, was conducted as well.

Fig. 7 shows for each of the differently heat-treated Co-Ni-Ga single crystals a superposition of two integrated 1D-line patterns obtained from the Bragg reflections on detector 1, which were recorded at -5% applied strain. The d-spacing range is limited to 1.2 – 1.8 Å in order to focus on the diffraction peaks of the (002) and (200) lattice planes. For further details on the data evaluation and extraction, the reader is referred to the supplementary material, where the procedure is exemplarily highlighted for the 300 °C aged condition. As already mentioned in chapter 2, for the sake of brevity, only diffraction data of detector 1 in backscattering direction are shown. All material states featured an austenitic cubic structure with space group Pm-3m (#221) in the unloaded condition at 100 °C (shown in the supplementary material). Upon loading, the stress-induced phase transformation from B2-austenite to $L1_0$-martensite occurred gradually, as already highlighted by the optical micrographs in Fig. 6. As can be deduced from Fig. 7, the transformation is completed and a fully martensitic microstructure is present upon loading to the maximum strain level within each single cycle test (end of the stress-strain "plateau"). Diffraction peaks being visible arise from the (200) and (002) lattice planes of stress-induced martensite. Diffraction data revealed

up to four martensite domain variants labeled as (V_1 – V_4). Reflections of the austenitic parent phase are fully vanished. The lattice correspondence of the domain variants will be detailed in section 4.1.1. The stress-induced martensite is indexed as a body-centered tetragonal (bct) structure with space group P4/mmm (#123) being in line with [6]. Apart from numerous additional reflections on the other detectors stemming from other lattice planes (cf. [6]), additional domain variants were not detected.

Table 1: Intensity ratios Ψ of CVP_A, CVP_B and CVP_A/CVP_B at -5% applied compressive strain for ⟨001⟩-oriented $Co_{49}Ni_{21}Ga_{30}$ single crystals in the solution-annealed condition and after aging for 3 h at 300 °C, 350 °C and 400 °C, respectively. Intensities of the martensite domain variants (V_1 – V_4) were calculated from the diffractograms shown in Fig. 7.

Intensity ratio Ψ [-]	Solution-annealed	3 h / 300 °C	3 h / 350 °C	3 h / 400 °C
$\Psi_{CVP_A} = V_2/V_1$	0.68	0.74	0.92	0.91
$\Psi_{CVP_B} = V_4/V_3$	-	0.79	0.92	-
$\Psi_{CVP_A/CVP_B} = (V_1+V_2)/(V_3+V_4)$	(∞)	5.8	2.2	(∞)

Twinning of the domain variant pairs V_1/V_2 and V_3/V_4 leads to correspondent variant pairs, i.e. CVP_A and CVP_B, respectively (cf. schematic in Fig. 7e). Based on the diffraction intensities, the volume fraction of the domain variant pair V_1/V_2 is higher than V_3/V_4. In the present study, individual domain variants and CVP systems are labeled in accordance to their volume fractions. The major domain within CVP_A and CVP_B is denoted as V_1 and V_3, respectively. Correspondingly, CVP_A is the dominant twin pair of stress-induced martensite in the samples investigated. The schematic in Fig. 7e demonstrates the relations on the nano-

and mesoscopic scale between the domain variants, the CVP systems and the types of HPVs observed in the heat treatment conditions. The diffraction peak intensities being visible in the diffractograms of Fig. 7a-d are in good agreement with the volume fraction of each domain variant. Thus, the CVP systems (CVP_A and CVP_B) can be associated with the martensite plates (types of HPVs) based on their respective volume fractions being visible in the optical micrographs (Fig. 6). Based on neutron diffraction data, the dominant group of martensite plates (called HPV_A) comprises the domain variant pair V_1/V_2 (i.e. CVP_A). Correspondingly, martensite plates with the second orientation and of minor volume fraction (called HPV_B) comprise the domain variant pair V_3/V_4 (i.e. CVP_B). In addition, analysis of the integrated diffraction peak intensities allows to quantitatively evaluate the actual twinning state. Calculated volume ratios are listed in Tab. 1.

As is obvious from the diffractograms the performed heat treatments strongly affect the transformation behavior in the Co-Ni-Ga system. In the solution-annealed condition (Fig. 7a), the martensitic phase merely consists of two domain variants. Thus, only one single, internally twinned CVP system, i.e. (CVP_A^{sol}), is present. In full agreement with the OM observations in Fig. 6a-c, the neutron diffraction data in Fig. 7b-d provide clear evidence for the presence of two different, internally twinned CVP systems, i.e. CVP_A and CVP_B, upon 300 and 350 °C aging, while the 400 °C aged sample is again characterized by the formation of only a single CVP system (CVP_A^{400}). However, the variant selection in the aged conditions featuring a configuration with two CVPs (300 and 350 °C) is not uniform, i.e. one CVP system is favored over the second one as shown in Tab. 1. The volume fraction of CVP_A^{350} is nearly two times higher than that of CVP_B^{350}, while CVP_A^{300} is favored over CVP_B^{300} by a factor of six. As already stated before, beside the number of existing CVP (HPV)

systems, this volume fraction distribution is consistent with the OM observations in Fig. 6. Furthermore, significant differences in the variant selection are not only existent between the CVP systems, but also among the twin-related domain variants forming an individual CVP. Tab. 1 shows a volume ratio of 0.68 within CVP_A of the solution-annealed sample (the inverse definition of the intensity ratios in comparison to the 3rd row has to be considered here). Aging at 300, 350 and 400 °C leads to increased values of 0.74, 0.92 and 0.91, respectively. CVP_B, where existing, is characterized by the same tendencies. Increased values clearly indicate an increase of the volume fraction of the minor domain variant at the expense of the major one, i.e. twinning.

4. Discussion of the results

4.1 Stress-induced martensitic transformation

As a consequence of MT, a single-crystalline structure of the austenitic parent phase transforms to a complex martensitic microstructure based on a shear type process. During the SIMT most favorable martensite variants nucleate and grow obeying the resolved shear stress criterion [14],[54],[55]. In general, the crystallographic orientation of the material, stress state, temperature and thermo-mechanical history were found to govern the selection of the martensite domain variants in the Co-Ni-Ga system [6],[13],[14],[33],[40]. In the following, the influence of a heat treatment on the SIMT, i.e. martensite variant selection and the morphology of martensite, will be discussed. Beforehand, theoretical considerations detailing the orientation relationships between the martensitic phase and the austenitic matrix will be introduced.

4.1.1 Crystallographic orientation relationships

From the crystallographic point of view, numerous models (Bain, Kurdjumow-Sachs, Nishiyama-Wassermann, Pitsch, and Greninger-Troiano) have been introduced to describe the orientation relationship between the austenitic and martensitic phase. In case of the Heusler-type Co-Ni-Ga alloy, the Bain model allows for a simplified description of the martensite variant distribution. As highlighted in Fig. 8a, three tetragonal bain-correspondent variant (BCV) orientations can result from the cubic-to-tetragonal MT with their extensional c-axes parallel to the main cubic axes of the parent B2-austenite. In the present study, i.e. during uniaxial compressive loading along ⟨001⟩ crystal direction, BCV_3 is energetically suppressed and only BCV_1 and BCV_2 with c-axes perpendicular to the loading direction can evolve. The CVP formation based on these two evolving BCVs is illustrated in Fig. 8b. Two possible twin configurations with twinning planes of type {110} prevail, i.e. both twinning events of the pair BCV_1/BCV_2 along (110) and $(\bar{1}10)$ lead to the formation of a single CVP system. Furthermore, the development of a coherent and stress-free twinning plane within a CVP necessitates a rotation of the martensite domain variants in relation to the original orientation of the BCVs. The rotation angle ± φ depends on the lattice parameters a and c. The two possible twin configurations (Fig. 8b) represent the CVP systems seen in the *in situ* experiments (cf. Fig. 6 and 7), i.e. CVP_A and CVP_B consisting of the martensite domain variants V_1/V_2 and V_3/V_4, respectively. In the neutron diffraction analysis conducted in present work, the occurrence of a CVP is related to the appearance of a pair of diffraction peaks resulting from (200) and (002) lattice planes of the corresponding twin-related domain variants (Fig. 7). In contrast, optical micrographs are only able to depict the traces of the habit planes. The habit planes of HPV_A and HPV_B are aligned to near (011),$(0\bar{1}1)$ and

(101),($\bar{1}$01) of austenite, respectively. This is in good agreement with the traces of the habit planes being inclined ~ ± 45° to the compression axis seen on the {100} lateral surfaces in Fig. 6.

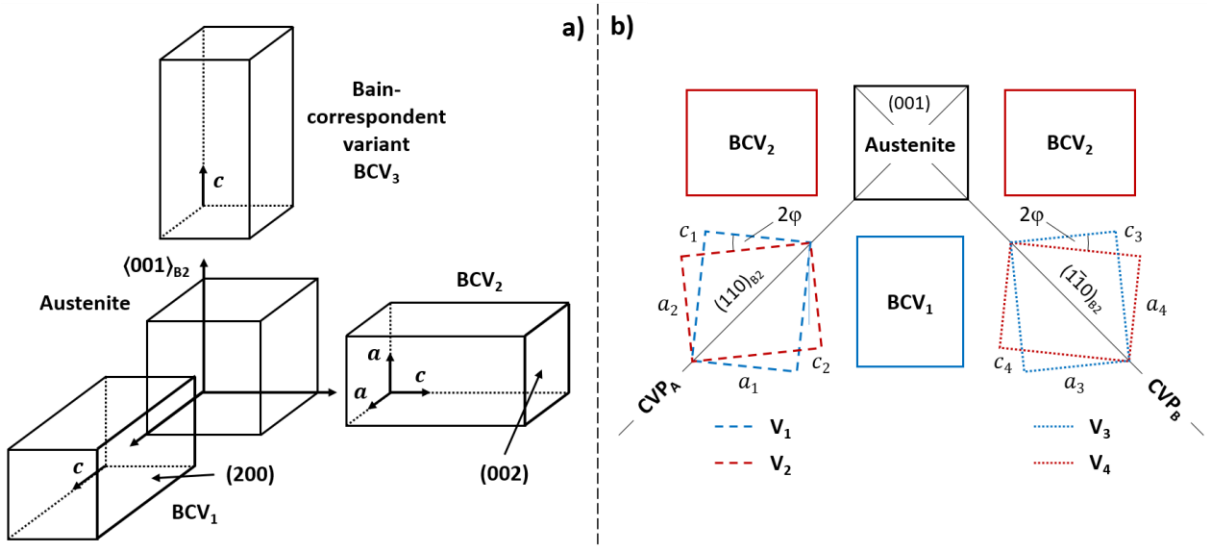

Figure 8: Bain correspondence of the three tetragonal martensite domain variant orientations to cubic austenite (a). Two possible twin configurations, i.e. CVP systems, with twinning planes of type {110} under compressive loading along ⟨001⟩ of the original austenite crystal (b). See main text for details.

4.1.2 Impact of heat treatment

The *in situ* analysis reveals a significant influence of the heat treatment on the SIMT. In previous work, the transformation behavior of solution-annealed ⟨001⟩-oriented $Co_{49}Ni_{21}Ga_{30}$ single-crystalline material under compressive load was studied via *in situ* OM [33]. In the precipitate-free condition, the stress-induced forward transformation is characterized by the nucleation and growth of a dominant martensite plate with well-defined habit planes. The *in situ* neutron diffraction analysis of present work confirms the formation

of a single, internally twinned CVP system (CVP_A^{sol} in Fig. 7a). Such kind of SIMT behavior characterized by only one dominant martensite plate has also been reported for as-grown Co-Ni-Ga [6],[40].

As is obvious from the micrographs 300, 350 and 400 °C aging treatments for 3 h evoke significant morphological differences in the martensitic phase. Here, it has to be emphasized that these significant differences in the transformation behavior in terms of the martensite variant selection and martensite morphology result from the aging-induced microstructural features, as explained in detail in the following. As is well known, in direct vicinity of the grips lateral constraints between the grips and the sample can affect the stress-induced transformation behavior observed by in situ OM. However, in the present work only representative areas from the midsection of the sample surfaces being not affected by lateral constraints were investigated (cf. inset in Fig.1). The precipitation of γ'-nanoparticles with spheroidal shape upon aging at 350 °C (Fig. 5b, c) promotes the evolution of two differently oriented types of martensite plates (2nd column of Fig. 6). The martensite plates are internally twinned comprising CVP_A^{350} and CVP_B^{350} as illustrated in Fig. 7c and e. This multi-variant martensite selection is in excellent agreement with previous results [33] for a condition containing spheroidal γ'-particles following an 350 °C aging treatment for 1 h. The twofold martensitic microstructure is supposed to result from coherency stress fields existing around the nanoparticles [33],[54]. Using a micro-mechanical model, Gall et al. [54] calculated local resolved shear stresses of coherent precipitates on the 24 CVP systems in Ni-Ti. Remarkable differences in the magnitude of the resolved shear stresses acting on the individual CVPs have been predicted. Thus, not all CVPs experience the same local stress state eventually leading to preferential nucleation sites for the MT [54]. In present work the dominant CVP

(CVP_A^{350}) is favored by the applied external stress. Thus, the second CVP system (CVP_B^{350}) is promoted by the superposition of the external and the precipitate-induced local stress fields. Further CVP systems cannot evolve under compression along the ⟨001⟩ orientation in the Co-Ni-Ga system owing to the crystallography of the cubic ⇌ tetragonal MT detailed above. Dadda et al. [40] also reported a complex multi-variant martensite morphology upon SIMT in ⟨001⟩-oriented as-grown Co-Ni-Ga at elevated temperatures above 120 °C. Pinning of propagating interfaces by diffusion of point defects, which is known as kinetic martensite stabilization [56], has been considered as the underlying microstructural mechanism. As can be deduced from the MT behavior of the solution-annealed condition [33], however, this mechanism is negligible here due to the hampered diffusion at the relative low test temperature of 100 °C.

Following aging at 300 °C, the TEM analysis in Fig. 5a reveals a single phase austenitic microstructure free of any secondary phases. Nonetheless, during the forward SIMT a twofold martensitic microstructure can be deduced from the 1st column of Fig. 6. Two differently oriented types of HPVs (HPV_A and HPV_B) being internally twinned (CVP_A^{300} and CVP_B^{300} in Fig. 7b) are present. Instead of γ'-nanoparticles, the 300 °C aging for 3 h is thought to form Guinier-Preston (G-P) zone-like clusters (not resolvable by TEM) due to enhanced diffusional atomic mobility [11],[23]. These clusters create small changes in atomic ordering, i.e. short-range order inhomogeneities, which can provide preferential nucleation sites for the MT [11]. However, as can be deduced from the analysis of the CVP volume fractions (3rd row in Tab. 1), CVP_A^{300} is preferred over CVP_B^{300} by a factor of six, while the 350 °C aged sample is characterized by an almost equal CVP distribution (factor of two). That means that

the effect of clusters on the evolution of the second CVP system is less pronounced than the strong local stress fields existing around the spheroidal γ'-particles.

The aging treatment at 400 °C for 3 h results in the precipitation of γ'-nanoparticles featuring an elongated shape with up to 40 nm length (Fig. 5d-f). In contrast to the twofold CVP configuration in the presence of spheroidal precipitates following the 350 °C aging, the SIMT of the 400 °C aged sample is predominantly characterized by martensite plates (HPVs) of a single orientation with respect to the loading direction (3rd column of Fig. 6). The martensite plates are internally twinned comprising CVP_A^{400} as illustrated in Fig. 7c and e. Thus, the coherency stress fields around the elongated particles do not promote the formation of the second CVP system. Actually, the magnitude of local stress fields around perfectly coherent precipitates increases with precipitate size [54]. In the Co-Ni-Ga system, Chumlyakov et al. [45] reported elongated particles with sizes up to 100 nm formed at temperatures as high as 600 °C, still keeping coherency with the surrounding matrix. This fact underlines the coherent character of the particles investigated in the present study. However, as Gall et al. [54] already noted in their study, the effect of the special dispersion of precipitates has to be considered in any model trying to predict the growth of martensite plates in an aged material. Particles with non-spheroidal shape, such as the elongated particles following the 400 °C aging, will yield strong position- and orientation-dependent stress fields. Furthermore, precipitate interactions have to be taken into account. Depending on interparticle distance, stress fields of neighboring precipitates can overlap each other. Eventually, this affects the local stress distribution, i.e. local stress fields acting on the CVP systems will either be strengthened, diminished or even annihilated [44],[54]. It is obvious from the *in situ* experiments that the coherency stress fields around the finely dispersed particles of

spheroidal and elongated shape differently affect the formation of the second CVP system, i.e. the martensite variant selection. In order to clarify the underlying microstructural mechanisms, precise modeling of the (local) position dependent resolved shear stresses on the individual CVPs is required.

Nonetheless, it is important to note that the transformation behavior of the 400 °C aged sample significantly differs from the solution-annealed condition [33], although both are characterized by the formation of a single CVP system (Fig. 7). In contrast to a single dominant martensite plate shown for the solution-annealed reference state in [33], each of the aforementioned aging treatments leads to an increased number of interfaces during the SIMT (Fig. 6). This refinement of the martensite morphology results from both difficulties in accommodating the martensite within the irregular stress fields around the G-P zones as well as the particles and an increase in elastic energy accumulation due to considerable elastic deformation of the non-transforming particles and the surrounding matrix [30],[31],[33]. However, the *in situ* OM analysis (Fig. 6) reveals that the segregation of large elongated γ'-particles upon aging at 400 °C seems to further refine the martensite morphology in comparison to the other aging treatments. A drastic reduction in twin thickness of thermally induced martensite has been already observed with increasing particle size in Co-Ni-Ga crystals [31]. Once a critical particle size is exceeded, additional micromodulations of the martensitic phase take place in order to accommodate the transformation strain [30],[31]. Although the nature of these micromodulations is not fully understood so far [31], the refinement of the thermally induced martensitic microstructure is in line with the micrographs of present work revealing the stress-induced martensitic morphology. Similar trends, i.e. a strong interrelationship between the martensitic morphology and the particle

size and/or interparticle distance, were established in Ni-Ti [57], Fe-based [58] and Cu-based SMAs [59].

4.2 Functional stability

A significant influence of uniaxial mechanical cycling under compression is visible on the stress-strain responses of Co-Ni-Ga single crystals shown in Fig. 3. In general, cyclic deformation can lead to a decrease of σ_{cr} and $\Delta\sigma$ as well as an accumulation of irrecoverable strains (ε_{irr}) (cf. Fig. 4). The degree of changes, however, is strongly dependent on the performed heat treatment. Previous work investigating the underlying microstructural mechanisms demonstrated that dislocation slip in the matrix is at the origin of this evolution of the transformation characteristics in the course of cycling in various SMA systems [13],[14],[34]–[37],[39],[47]. Dislocations are known to be formed at the interphase boundaries during SIMT in order to accommodate the mismatch in crystal structure between the austenitic and martensitic phase [60]–[62]. On the one hand, the accumulation of residual strains stems from slip deformation and retained martensite. Localized stress fields around the dislocation arrangements provide mechanical energy being capable to stabilize the stress-induced martensite [34],[36],[47]. On the other hand, the decrease in σ_{cr} with increasing cycle number is attributed to internal stress fields associated with both dislocation formation and retained martensite, if existent. Eventually, these stress fields facilitate the nucleation of martensite in subsequent cycles. In turn, the evolution of $\Delta\sigma$ is dominated by the decreasing trend of σ_{cr} [35],[37]. Activation of multiple martensite variants during SIMT has been reported to promote higher dislocation activity and more intense cyclic degradation of the functional properties [13],[47]. Dislocation activity and, thus, cyclic stability is strongly dependent on crystallographic orientation [14],[35],[36], stress state (tension vs.

compression) [13],[35], test temperature [13],[34], and heat treatment [34]–[36],[63]. Regarding the latter, variations in particle size significantly affect the cyclic behavior of SMAs. Improved functional stability was shown for reduced particle sizes [36],[63]. As will be detailed in the following, the present results are fully consistent with those findings.

The ⟨001⟩-oriented Co-Ni-Ga crystal in the solution-annealed condition demonstrates the highest resistance to cyclic degradation (Fig. 3 and 4). Both the Schmid factor for dislocation slip due to an externally applied stress as well as the RSSF for the MT play an important role with respect to the fatigue behavior [36],[64]. The favorable orientation for the MT associated with easy motion of the martensitic interface and the lack of available slip systems provide rational for the excellent performance in the ⟨001⟩-oriented reference state [14]. Perfect recoverability upon cycling nearly without any irrecoverable strain accumulation is visible in Fig. 3, while the slight decrease in σ_{cr} is supposed to result from minor dislocation generation induced by the moving martensite interfaces. Such excellent cyclic properties of ⟨001⟩-oriented single-crystalline material were already reported for the as-grown state under tensile and compressive loading at 100 °C [13].

Enhanced cyclic stability, i.e. only minor changes of the stress-strain hysteresis with cycling, were also observed in present work following aging treatments at 300 and 350 °C for 3 h. As proposed in several studies, martensite variant interactions should lead to a more pronounced pile-up of dislocations in the vicinity of austenite-martensite phase boundaries [13],[47]. Consequently, the configuration with two CVPs associated with multiple interfaces in the 300 and 350 °C aged conditions (Fig. 6 and 7) is supposed to be the origin of the more intensified decrease of σ_{cr} after 700 SE cycles in relation to the solution-annealed state (Fig. 4). Nonetheless, the dislocation activity in both aging conditions is not capable to

induce severe transformation irreversibilities, i.e. mechanical stabilization of martensite in particular. Almost perfect recoverability during repeated SIMT with only marginal accumulation of irrecoverable strains (Fig. 3 and 4) is still present. Eventually, it can be stated that the martensite variant selection is of minor importance for the functional stability of the SE effect in the ⟨001⟩ crystallographic orientation.

In consequence, it is concluded that the interaction between moving martensite plates and precipitates is of highest importance in aged Co-Ni-Ga material. Although for the 400 °C aged single crystal the SIMT is characterized by the formation of martensite plates with the same orientation only (Fig. 7), a pronounced change of the stress-strain curves with cycling can be observed in presence of the large elongated γ'-particles (Fig. 5d-f). Noteworthy, all transformation characteristics steadily change over the 700 SE cycles following the 400 °C aging, while in the other conditions relevant values evolve quite rapidly during the first cycles followed by saturation (cf. Fig. 4). Cyclic saturation of the transformation characteristics is usually observed in SMAs [13],[14],[36],[63] and is attributed to a steady-state dislocation structure, which no longer changes with further cycling [37]. In Fe-Ni-Co-Al-Ta SMAs, Krooß et al. [47] found a significant amount of mechanically stabilized martensite in the vicinity of finely dispersed precipitates after SE cycling and concluded that this mechanism substantially contributes to the evolution of irrecoverable strains. Kireeva et al. [30] already reported initial traces of irreversibility in Co-Ni-Ga containing elongated γ'-particles, i.e. the same particle configuration as in the 400 °C aged condition of present work. The authors found residual tiny martensite plates and dislocation formation due to pronounced martensite-precipitate interactions after monotonic SE testing. Considering a higher number of cycles, consequently, these interactions are supposed to lead to an intensive pile-up of

dislocations in direct vicinity of the large elongated particles in case of the 400 °C aged condition. Here, the dislocation-controlled degradation mechanisms cause the significant evolution of the stress-strain behavior with cycling (Fig. 4). Clearly, the stress level for the forward transformation (σ_{cr}) steadily decreases with increasing cycle number, while the effect of cyclic loading on the stress level for the reverse transformation ($\sigma_{cr,rev}$) is less pronounced for all heat treatments considered (cf. Fig. 3). This asymmetric evolution of the critical stress levels being well-known from literature [14],[37] governs the decrease of $\Delta\sigma$ during cycling, this being highlighted in Fig. 4.

The severe irreversible processes associated with the large particles are also in line with the large hysteresis of the 400 °C aged single crystal in the first cycle. Gall et al. [36] as well as Krooß et al. [63] found in NiTi and Fe-Ni-Co-Al-Ta SMAs, respectively, a correlation between the inherent hysteresis width and the fatigue performance of the studied materials. For a larger hysteresis $\Delta\sigma$ they found a more severe evolution of the transformation behavior during SE cycling. This is in good agreement with the results of present work. Nonetheless, even if the changes of the transformation behavior become more pronounced with increasing aging temperature and hysteresis width (Fig. 4), the 350 °C aged condition containing small spheroidal particles is still characterized by superior cyclic stability regardless of the increase of $\Delta\sigma$ by a factor of about 4 compared to the solution-annealed condition. Given the above observations, the present results indicate that the particle morphology controls unambiguously the evolution of the stress-strain response in the course of cycling and eventually the fatigue performance. While the excellent resistance against cyclic degradation of the ⟨001⟩ orientation is maintained in the presence of small γ'-particles after the 350 °C aging, the precipitation of large elongated particles leads to pronounced irreversible

processes and, thus, poor cyclic performance. Such a relationship between the fatigue resistance and particle size has been reported in Ni-Ti and Fe-Ni-Co-Al-Ta SMA systems as well [35],[36],[63]. Again, the large particles in the 400 °C aged condition not only lead to a pronounced hysteresis expansion, but also to a significant increase of σ_{cr} associated with higher stress levels during SE testing compared to the other heat treatment conditions (Fig. 3). Higher stresses are known to promote plastic deformation and defect generation. However, it should be mentioned that the stress levels of around -900 MPa reached are still below the stress, which is required for slip in the martensitic phase of ⟨001⟩-oriented single crystals [6] eventually rationalizing the dominant role of the precipitate structure on the functional properties.

Based on the results obtained within this work, Fig. 9 highlights the morphology of the stress-induced martensitic forward transformation under compressive SE loading and essential microstructural features, which eventually control the functional properties in ⟨001⟩-oriented single-crystalline Co-Ni-Ga SMA depending on the given heat treatment. The schematic is designed in such way that it directly can be compared to the TEM and *in situ* optical micrographs in Fig. 5 and 6, respectively. The main findings of present work (as already presented and discussed above) are briefly summarized in the following to allow for rapid access to the mechanisms detailed in the schematic. Furthermore, most important aspects deduced from single cycle tests (detailed in the supplementary material) are considered for assessment of results (cf. definitions provided in Fig. 1):

The solution-annealed and precipitate-free reference state is characterized by a narrow stress hysteresis width and excellent resistance against cyclic degradation. The easy motion of a dominant martensite plate during SIMT is associated with only minor irreversible processes

(Fig. 9a). In turn, the multiple interface microstructure after aging at 300 and 350 °C for 3 h is at the origin of pronounced strain hardening during the forward transformation and stress hysteresis widening with increasing aging temperature. GP zone-like clusters (Fig. 9b) and spheroidal γ'-particles with diameters of up to 10 nm (Fig. 9c) are preferential nucleation sites for the SIMT leading to the formation of a twofold HPV configuration (cf. orientations of the dark and light gray plates in Fig. 9b and c). Interactions between these interfaces, especially in the 350 °C aged condition (visualized by hachured areas in Fig. 9c), hamper phase boundary motion and promote dislocation activity (visualized by the amount of dislocation structures in Fig. 9a-c). In addition, the spheroidal γ'-particles (350 °C) are effective obstacles during SIMT leading to a more pronounced hysteresis expansion compared to the 300 °C aged material state. Nonetheless, both aging treatments still feature enhanced functional stability with excellent recoverability of the SIMT upon cycling. On the contrary, the coherency stress fields existing around large elongated γ'-particles of up to 40 nm length do not promote the formation of two differently oriented HPVs (Fig. 9d). However, a further refinement of the martensitic morphology is caused in comparison to the other aging treatments (visualized by width of the martensite plates in Fig. 9). Furthermore, these larger precipitates are strong obstacles for movement of the phase boundaries. Thereby, an intensive pile-up of dislocations is assumed to occur near the elongated particles during SIMT leading to a drastic expansion of the stress hysteresis and finally poor cyclic performance. Consequently, the particle morphology seems to be of utmost importance for the phase transformation behavior and functional properties.

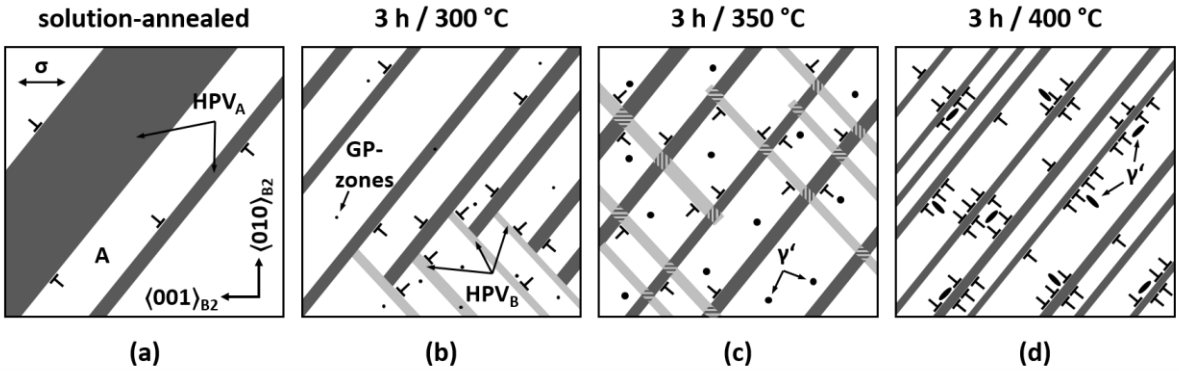

Figure 9: Schematic illustrating the microstructural features, i.e. the martensitic morphology during forward SIMT under compression, secondary phases and severity of dislocation formation, of ⟨001⟩-oriented $Co_{49}Ni_{21}Ga_{30}$ single crystals in the solution-annealed condition [33] (a) and after aging for 3 h at 300 °C (b), 350 °C (c) and 400 °C (d), respectively. Lateral surfaces of type (100) with loading direction in ⟨001⟩ crystal direction being horizontal are shown. Martensite plates are depicted in dark (HPV_A) and light (HPV_B) gray. Aging treatments promote formation of GP zone-like clusters (b) as well as precipitation of spheroidal (c) and elongated (d) γ'-particles. For further details, see main text.

The results clearly show that with respect to long-term stability aging parameters have be to carefully controlled in the Co-Ni-Ga system. Obviously, the precipitate structure is a key criterion for assessment of the functional fatigue behavior. The activation of a multi-variant martensitic microstructure during repeated SIMT is found to be of minor importance only. This is in contrast to results reported elsewhere [13],[47]. In part, such differences can be attributed to the hampered dislocation activity in the crystallographic orientation being studied in present work. Clearly, future work including other crystallographic orientations and loading under tension has to be accomplished to fully understand the fatigue behavior in aged Co-Ni-Ga. In particular, the investigation of orientations favorably oriented for

dislocation motion will provide more insights into the role of both a multi-variant SIMT and the strength-enhancing effect of finely dispersed nanoparticles on the cyclic degradation behavior.

5. Conclusions

In present work, the effect of aging treatments on the stress-induced formation of martensite and the stability of the functional properties in single-crystalline $Co_{49}Ni_{21}Ga_{30}$ (at.%) SMAs were investigated. Using TEM analysis the presence and morphology, i.e. size and shape, of the nanometric secondary γ'-phase were assessed. Isothermal superelastic (SE) compression tests accompanied by *in situ* techniques, i.e. optical microscopy (OM) and neutron diffraction, were conducted in order to investigate systematically the transformation behavior, focusing on the martensite variant selection and martensite morphology. The results obtained in present work can be summarized as follows:

1. Aging treatments performed at 300, 350 and 400 °C for 3 h lead to mutually different microstructures in Co-Ni-Ga single crystals. Spheroidal γ'-precipitates with diameters up to 10 nm are formed after aging at 350 °C, while aging at 400 °C results in the formation of elongated particles of 40 nm average length. TEM analysis indicates that after 300°C aging, an austenitic single phase microstructure is present. However, it seems reasonable to assume that minor changes in atomic ordering, i.e. short-range order inhomogeneities, evolve.

2. The martensite morphology as well as the variant selection strongly depend on the aging treatments. In the case of minor changes in atomic ordering (300 °C) and evolution of spheroidal particles (350 °C), the formation of two differently oriented internally twinned types of HPVs, i.e. the occurrence of two CVP systems, is observed. The effect of the

spheroidal particles on the evolution of the second CVP system is stronger than that of short-range order phenomena. In contrast, the coherency stress fields existing around the elongated particles (400 °C) do not promote the second CVP system and, thus, only a single type of internally twinned martensite is present.

3. The ⟨001⟩ crystallographic orientation features an excellent resistance against cyclic degradation. However, aging treatments can significantly affect the evolution of the stress-strain response under SE cycling in compression. The results obtained in present work clearly demonstrate that, in particular, the particle morphology is of utmost importance with respect to irreversibility and associated fatigue properties. When minor changes in atomic ordering and spheroidal particles after aging at 300 and 350 °C, respectively, are present, the transformation behavior is characterized by enhanced cyclic stability with nearly perfect recoverability of the stress-induced martensitic transformation up to 700 cycles. In contrast, 400 °C aging results in the formation of larger elongated γ'-particles. This condition shows poor cyclic performance.

Acknowledgements

This work was supported by Deutsche Forschungsgemeinschaft (DFG) through the dislocated research group FOR 1766. The authors from Russia acknowledge funding from the Ministry of Science and Education of Russian Federation. The authors gratefully acknowledge the assistance of Keith Allum (ISIS neutron source, Oxfordshire), Thomas Pham, Michael Wiegand and Christoph Pohlmann with the experiments.

References

[1] D.C. Lagoudas, Shape memory alloys: Modeling and engineering applications, 2008.

[2] K. Otsuka (Ed.), Shape memory materials, 1st ed., Cambridge University Press, Cambridge, 1999.
[3] K. Otsuka, X. Ren, Physical metallurgy of Ti–Ni-based shape memory alloys, Progress in Materials Science 50 (2005) 511–678.
[4] T.W. Duerig, K.N. Melton, D. Stöckel, Engineering Aspects of Shape Memory Alloys, Elsevier Science, Burlington, 1990.
[5] M.H. Elahinia, M. Hashemi, M. Tabesh, S.B. Bhaduri, Manufacturing and processing of NiTi implants, Progress in Materials Science 57 (2012) 911–946.
[6] A. Reul, C. Lauhoff, P. Krooß, M.J. Gutmann, P.M. Kadletz, Y.I. Chumlyakov, T. Niendorf, W.W. Schmahl, In Situ Neutron Diffraction Analyzing Stress-Induced Phase Transformation and Martensite Elasticity in [001]-Oriented $Co_{49}Ni_{21}Ga_{30}$ Shape Memory Alloy Single Crystals, Shape Memory and Superelasticity 4 (2018) 61–69.
[7] K. Oikawa, T. Ota, Y. Imano, T. Omori, R. Kainuma, K. Ishida, Phase equilibria and phase transformation of Co−Ni−Ga ferromagnetic shape memory alloy system, Journal of Phase Equilibria and Diffusion 27 (2006) 75–82.
[8] M. Wuttig, J. Li, C. Craciunescu, A new ferromagnetic shape memory alloy system, Scripta Materialia 44 (2001) 2393–2397.
[9] K. Oikawa, T. Ota, F. Gejima, T. Ohmori, R. Kainuma, K. Ishida, Phase Equilibria and Phase Transformations in New B2-type Ferromagnetic Shape Memory Alloys of Co-Ni-Ga and Co-Ni-Al Systems, Materials Transactions 42 (2001) 2472–2475.
[10] P. Krooß, P.M. Kadletz, C. Somsen, M.J. Gutmann, Y.I. Chumlyakov, W.W. Schmahl, H.J. Maier, T. Niendorf, Cyclic Degradation of $Co_{49}Ni_{21}Ga_{30}$ High-Temperature Shape Memory Alloy, Shape Memory and Superelasticity 2 (2016) 37–49.
[11] J.A. Monroe, I. Karaman, H.E. Karaca, Y.I. Chumlyakov, H.J. Maier, High-temperature superelasticity and competing microstructural mechanisms in $Co_{49}Ni_{21}Ga_{30}$ shape memory alloy single crystals under tension, Scripta Materialia 62 (2010) 368–371.
[12] J. Dadda, H.J. Maier, I. Karaman, H.E. Karaca, Y.I. Chumlyakov, Pseudoelasticity at elevated temperatures in [001] oriented $Co_{49}Ni_{21}Ga_{30}$ single crystals under compression, Scripta Materialia 55 (2006) 663–666.
[13] P. Krooß, T. Niendorf, P.M. Kadletz, C. Somsen, M.J. Gutmann, Y.I. Chumlyakov, W.W. Schmahl, G. Eggeler, H.J. Maier, Functional Fatigue and Tension–Compression Asymmetry in [001]-Oriented $Co_{49}Ni_{21}Ga_{30}$ High-Temperature Shape Memory Alloy Single Crystals, Shape Memory and Superelasticity 1 (2015) 6–17.
[14] J. Dadda, H.J. Maier, D. Niklasch, I. Karaman, H.E. Karaca, Y.I. Chumlyakov, Pseudoelasticity and Cyclic Stability in $Co_{49}Ni_{21}Ga_{30}$ Shape-Memory Alloy Single Crystals at Ambient Temperature, Metallurgical and Materials Transactions A 39 (2008) 2026–2039.
[15] C. Lauhoff, M. Vollmer, P. Krooß, I. Kireeva, Y.I. Chumlyakov, T. Niendorf, Pathways Towards Grain Boundary Engineering for Improved Structural Performance in Polycrystalline Co–Ni–Ga Shape Memory Alloys, Shape Memory and Superelasticity 5 (2019) 73–83.
[16] M. Vollmer, P. Krooß, C. Segel, A. Weidner, A. Paulsen, J. Frenzel, M. Schaper, G. Eggeler, H.J. Maier, T. Niendorf, Damage evolution in pseudoelastic

polycrystalline Co–Ni–Ga high-temperature shape memory alloys, Journal of Alloys and Compounds 633 (2015) 288–295.
[17] E. Karsten, G. Gerstein, O. Golovko, A. Dalinger, C. Lauhoff, P. Krooss, T. Niendorf, A. Samsonenko, H.J. Maier, Tailoring the Microstructure in Polycrystalline Co–Ni–Ga High-Temperature Shape Memory Alloys by Hot Extrusion, Shape Memory and Superelasticity 5 (2019) 84–94.
[18] T. Niendorf, C. Lauhoff, E. Karsten, G. Gerstein, A. Liehr, P. Krooß, H.J. Maier, Direct microstructure design by hot extrusion – High-temperature shape memory alloys with bamboo-like microstructure, Scripta Materialia 162 (2019) 127–131.
[19] C. Lauhoff, A. Fischer, C. Sobrero, A. Liehr, P. Krooß, F. Brenne, J. Richter, M. Kahlert, S. Böhm, T. Niendorf, Additive Manufacturing of Co-Ni-Ga High-Temperature Shape Memory Alloy, Metallurgical and Materials Transactions A 51 (2020) 1056–1061.
[20] C. Lauhoff, N. Sommer, M. Vollmer, G. Mienert, P. Krooß, S. Böhm, T. Niendorf, Excellent superelasticity in a Co-Ni-Ga high-temperature shape memory alloy processed by directed energy deposition, Materials Research Letters 8 (2020) 314–320.
[21] J. Liu, M. Xia, Y. Huang, H. Zheng, J. Li, Effect of annealing on the microstructure and martensitic transformation of magnetic shape memory alloys CoNiGa, Journal of Alloys and Compounds 417 (2006) 96–99.
[22] T. Niendorf, P. Krooß, C. Somsen, G. Eggeler, Y.I. Chumlyakov, H.J. Maier, Martensite aging – Avenue to new high temperature shape memory alloys, Acta Materialia 89 (2015) 298–304.
[23] E. Dogan, I. Karaman, Y.I. Chumlyakov, Z.P. Luo, Microstructure and martensitic transformation characteristics of CoNiGa high temperature shape memory alloys, Acta Materialia 59 (2011) 1168–1183.
[24] C. Lauhoff, P. Krooß, D. Langenkämper, C. Somsen, G. Eggeler, I. Kireeva, Y.I. Chumlyakov, T. Niendorf, Martensite aging in 〈001〉 oriented $Co_{49}Ni_{21}Ga_{30}$ single crystals in tension, Functional Materials Letters 11 (2018) 1850024.
[25] P.M. Kadletz, P. Krooß, Y.I. Chumlyakov, M.J. Gutmann, W.W. Schmahl, H.J. Maier, T. Niendorf, Martensite stabilization in shape memory alloys - Experimental evidence for short-range ordering, Materials Letters 159 (2015) 16–19.
[26] X. Ren, K. Otsuka, Origin of rubber-like behaviour in metal alloys, Nature 389 (1997) 579–582.
[27] J. Liu, H. Xie, Y. Huo, H. Zheng, J. Li, Microstructure evolution in CoNiGa shape memory alloys, Journal of Alloys and Compounds 420 (2006) 145–157.
[28] A.M. Zak, W. Dudzinski, Microstructural and In Situ Lorentz TEM Domain Characterization of As-Quenched and γ'-Precipitated $Co_{49}Ni_{30}Ga_{21}$ Monocrystal, Crystals 10 (2020) 153.
[29] G. Gerstein, V.A. L'vov, A. Kosogor, H.J. Maier, Internal pressure as a key thermodynamic factor to obtain high-temperature superelasticity of shape memory alloys, Materials Letters 210 (2018) 252–254.
[30] I.V. Kireeva, C. Picornell, J. Pons, I.V. Kretinina, Y.I. Chumlyakov, E. Cesari, Effect of oriented γ′ precipitates on shape memory effect and superelasticity in Co–Ni–Ga single crystals, Acta Materialia 68 (2014) 127–139.

[31] I.V. Kireeva, J. Pons, C. Picornell, Y.I. Chumlyakov, E. Cesari, I.V. Kretinina, Influence of γ′ nanometric particles on martensitic transformation and twinning structure of L10 martensite in Co–Ni–Ga ferromagnetic shape memory single crystals, Intermetallics 35 (2013) 60–66.
[32] Y.I. Chumlyakov, I.V. Kireeva, E.Y. Panchenko, V.A. Kirillov, E.E. Timofeeva, I.V. Kretinina, Y.N. Danil'son, I. Karaman, H. Maier, E. Cesari, Thermoelastic martensitic transformations in single crystals with disperse particles, Russian Physics Journal 54 (2012) 937–950.
[33] C. Lauhoff, A. Reul, D. Langenkämper, P. Krooß, C. Somsen, M.J. Gutmann, I. Kireeva, Y.I. Chumlyakov, W.W. Schmahl, T. Niendorf, Effect of nanometric γ′-particles on the stress-induced martensitic transformation in ⟨001⟩ -oriented $Co_{49}Ni_{21}Ga_{30}$ shape memory alloy single crystals, Scripta Materialia 168 (2019) 42–46.
[34] S. Miyazaki, T. Imai, Y. Igo, K. Otsuka, Effect of cyclic deformation on the pseudoelasticity characteristics of Ti-Ni alloys, Metallurgical Transactions A 17 (1986) 115–120.
[35] H. Sehitoglu, R. Anderson, I. Karaman, K. Gall, Y. Chumlyakov, Cyclic deformation behavior of single crystal NiTi, Materials Science and Engineering: A 314 (2001) 67–74.
[36] K. Gall, H.J. Maier, Cyclic deformation mechanisms in precipitated NiTi shape memory alloys, Acta Materialia 50 (2002) 4643–4657.
[37] A. Yawny, M. Sade, G. Eggeler, Pseudoelastic cycling of ultra-fine-grained NiTi shape-memory wires, Zeitschrift für Metallkunde 96 (2005) 608–618.
[38] G. Eggeler, E. Hornbogen, A. Yawny, A. Heckmann, M. Wagner, Structural and functional fatigue of NiTi shape memory alloys, Materials Science and Engineering: A 378 (2004) 24–33.
[39] R. Delville, B. Malard, J. Pilch, P. Sittner, D. Schryvers, Transmission electron microscopy investigation of dislocation slip during superelastic cycling of Ni–Ti wires, International Journal of Plasticity 27 (2011) 282–297.
[40] J. Dadda, H.J. Maier, I. Karaman, Y. Chumlyakov, High-temperature in-situ microscopy during stress-induced phase transformations in $Co_{49}Ni_{21}Ga_{30}$ shape memory alloy single crystals, International Journal of Materials Research 101 (2010) 1–11.
[41] H. Mughrabi, R.W. Cahn (Eds.), Plastic deformation and fracture of materials, Wiley-VCH, Weinheim, 1993.
[42] D.A. Keen, M.J. Gutmann, C.C. Wilson, SXD – the single-crystal diffractometer at the ISIS spallation neutron source, Journal of Applied Crystallography 39 (2006) 714–722.
[43] M. Hofmann, R. Schneider, G.A. Seidl, J. Rebelo-Kornmeier, R.C. Wimpory, U. Garbe, H.-G. Brokmeier, The new materials science diffractometer STRESS-SPEC at FRM-II, Physica B: Condensed Matter 385-386 (2006) 1035–1037.
[44] I.V. Kireeva, Z.V. Pobedennaya, Y.I. Chumlyakov, J. Pons, E. Cesari, I. Karaman, Effect of orientation on the high-temperature superelasticity in $Co_{49}Ni_{21}Ga_{30}$ single crystals, Technical Physics Letters 35 (2009) 186–189.
[45] Y.I. Chumlyakov, I.V. Kireeva, E.Y. Panchenko, E.E. Timofeeva, Z.V. Pobedennaya, S.V. Chusov, I. Karaman, H. Maier, E. Cesari, V.A. Kirillov,

High-temperature superelasticity in CoNiGa, CoNiAl, NiFeGa, and TiNi monocrystals, Russian Physics Journal 51 (2008) 1016–1036.
[46] D. Niklasch, J. Dadda, H.J. Maier, I. Karaman, Magneto-microstructural coupling during stress-induced phase transformation in $Co_{49}Ni_{21}Ga_{30}$ ferromagnetic shape memory alloy single crystals, Journal of Material Science 43 (2008) 6890–6901.
[47] P. Krooß, C. Somsen, T. Niendorf, M. Schaper, I. Karaman, Y. Chumlyakov, G. Eggeler, H.J. Maier, Cyclic degradation mechanisms in aged FeNiCoAlTa shape memory single crystals, Acta Materialia 79 (2014) 126–137.
[48] W. Abuzaid, Y. Wu, R. Sidharth, F. Brenne, S. Alkan, M. Vollmer, P. Krooß, T. Niendorf, H. Sehitoglu, FeMnNiAl Iron-Based Shape Memory Alloy: Promises and Challenges, Shape Memory and Superelasticity 5 (2019) 263–277.
[49] H. Sitepu, W.W. Schmahl, J.K. Allafi, G. Eggeler, A. Dlouhy, D.M. Toebbens, M. Tovar, Neutron diffraction phase analysis during thermal cycling of a Ni-rich NiTi shape memory alloy using the Rietveld method, Scripta Materialia 46 (2002) 543–548.
[50] P. Molnár, P. Šittner, V. Novák, P. Lukáš, Twinning processes in Cu–Al–Ni martensite single crystals investigated by neutron single crystal diffraction method, Materials Science and Engineering: A 481-482 (2008) 513–517.
[51] A.P. Stebner, S.C. Vogel, R.D. Noebe, T.A. Sisneros, B. Clausen, D.W. Brown, A. Garg, L.C. Brinson, Micromechanical quantification of elastic, twinning, and slip strain partitioning exhibited by polycrystalline, monoclinic nickel–titanium during large uniaxial deformations measured via in-situ neutron diffraction, Journal of the Mechanics and Physics of Solids 61 (2013) 2302–2330.
[52] G.K. Kannarpady, A. Bhattacharyya, M. Wolverton, D.W. Brown, S.C. Vogel, S. Pulnev, Phase quantification during pseudoelastic cycling of Cu–13.1Al–4.0Ni (wt.%) single-crystal shape memory alloys using neutron diffraction, Acta Materialia 56 (2008) 4724–4738.
[53] P.J. Brown, B. Dennis, J. Crangle, T. Kanomata, M. Matsumoto, K.-U. Neumann, L.M. Justham, K.R.A. Ziebeck, Stability of martensitic domains in the ferromagnetic alloy Ni_2MnGa, Journal of Physics: Condensed Matter 16 (2004) 65–75.
[54] K. Gall, H. Sehitoglu, Y.I. Chumlyakov, I.V. Kireeva, H.J. Maier, The Influence of Aging on Critical Transformation Stress Levels and Martensite Start Temperatures in NiTi, Journal of Engineering Materials and Technology 121 (1999) 19–27.
[55] K. Gall, H. Sehitoglu, Y.I. Chumlyakov, I.V. Kireeva, Tension–compression asymmetry of the stress–strain response in aged single crystal and polycrystalline NiTi, Acta Materialia 47 (1999) 1203–1217.
[56] S. Kustov, J. Pons, E. Cesari, J. van Humbeeck, Pinning-induced stabilization of martensite, Acta Materialia 52 (2004) 3083–3096.
[57] M. Nishida, C.M. Wayman, A. Chiba, Electron microscopy studies of the martensitic transformation in an aged Ti-51at%Ni shape memory alloy, Metallography 21 (1988) 275–291.
[58] J. Ma, B.C. Hornbuckle, I. Karaman, G.B. Thompson, Z.P. Luo, Y.I. Chumlyakov, The effect of nanoprecipitates on the superelastic properties of FeNiCoAlTa shape memory alloy single crystals, Acta Materialia 61 (2013) 3445–3455.
[59] J. Pons, E. Cesari, Martensitic transformation cycling in a β Cu-Zn-Al alloy containing γ-precipitates, Acta Metallurgica et Materialia 41 (1993) 2547–2555.

[60] J. Zhang, C. Somsen, T. Simon, X. Ding, S. Hou, S. Ren, X. Ren, G. Eggeler, K. Otsuka, J. Sun, Leaf-like dislocation substructures and the decrease of martensitic start temperatures: A new explanation for functional fatigue during thermally induced martensitic transformations in coarse-grained Ni-rich Ti–Ni shape memory alloys, Acta Materialia 60 (2012) 1999–2006.
[61] T. Simon, A. Kröger, C. Somsen, A. Dlouhy, G. Eggeler, On the multiplication of dislocations during martensitic transformations in NiTi shape memory alloys, Acta Materialia 58 (2010) 1850–1860.
[62] D.M. Norfleet, P.M. Sarosi, S. Manchiraju, M.F.-X. Wagner, M.D. Uchic, P.M. Anderson, M.J. Mills, Transformation-induced plasticity during pseudoelastic deformation in Ni–Ti microcrystals, Acta Materialia 57 (2009) 3549–3561.
[63] P. Krooß, T. Niendorf, I. Karaman, Y. Chumlyakov, H.J. Maier, Cyclic deformation behavior of aged FeNiCoAlTa single crystals, Functional Materials Letters 05 (2012) 1250045.
[64] K. Gall, H. Sehitoglu, R. Anderson, I. Karaman, Y.I. Chumlyakov, I.V. Kireeva, On the mechanical behavior of single crystal NiTi shape memory alloys and related polycrystalline phenomenon, Materials Science and Engineering: A 317 (2001) 85–92.

Autorenversion von: C. Lauhoff, A. Reul, D. Langenkämper, P. Krooß, C. Somsen, M.J. Gutmann, B. Pedersen, I.V. Kireeva, Y.I. Chumlyakov, G. Eggeler, W.W. Schmahl, T. Niendorf. Effects of aging on the stress-induced martensitic transformation and cyclic superelastic properties in Co-Ni-Ga shape memory alloy single crystals under compression, Acta Materialia, Volume 226, 2022, 117623, EISSN 1873-2453, https://doi.org/10.1016/j.actamat.2022.117623